PCCP

Accepted Manuscript

ROYAL SOCIETY OF CHEMISTRY

www.rsc.org/pccp

New insights into the mixing of gold and copper in nanoparticle by structural study of Au-Cu nanoalloys synthesized via wet chemistry method and pulsed laser deposition

Hélène Prunier[1], Jaysen Nelayah[1], Christian Ricolleau[1,*], Guillaume Wang[1], Sophie Nowak[2], Anne-Félicie Lamic-Humblot[3] and Damien Alloyeau[1]

[1] Laboratoire Matériaux et Phénomènes Quantiques (MPQ), UMR 7162 CNRS & Université Paris-Diderot, Bâtiment Condorcet, 4 rue Elsa Morante, 75205 Paris Cedex 13, France.

[2] UFR Chimie, Plateforme de caractérisation par rayons X, Université Paris Diderot, Bâtiment Lamarck B, 35 rue Hélène Brion, 75205 Paris Cedex 13, France.

[3] Laboratoire de Réactivité de Surface, UMR CNRS 7197, UPMC Université Paris 6, 4 Place Jussieu 75005 Paris, France.

* Corresponding author: christian.ricolleau@univ-paris-diderot.fr

Abstract

Gold-copper nanoparticles (Au-Cu NPs) were elaborated by both chemical (polyol reduction method) and physical (laser deposition) routes. The size, composition and crystal structure of these bimetallic nanoalloys were then characterized by aberration corrected transmission electron microscopy (TEM). Using a one-pot polyol method, Au-Cu nanocubes (NCs) with nominal compositions Au_3Cu and $AuCu_3$ were synthesized. The size and composition of the NCs were tuned by varying the amount and ratio of the Au(III) and Cu(II) ions used as metallic precursors in the reaction. While particle shape and size were well-controlled, single particle X-ray spectroscopy showed that, irrespective of the targeted compositions, the Cu content in all NCs was about 11-12 at. %, i.e. in both samples, the real composition was different from the nominal one. This was ascribed to an incompletely alloying of the two constituent metals of the alloy in the cubes due to the different reduction kinetics of the two metallic precursors. To shed light on the alloying of gold and copper at the nanoscale, Au-Cu NPs with targeted compositions Au_3Cu and $AuCu_3$ were deposited on amorphous carbon by laser ablation of two monometallic sources and their structural properties studied by TEM. These studies show that Au-Cu nanoalloys were synthesized in both samples and that the complete mixing of Au and Cu atoms achieved with this synthesis technique led to the production of Au-Cu NPs with well-controlled compositions. These results constitute a first but major step towards a complete understanding of the details of the kinetics and thermodynamics determining the mixing of gold and copper atoms at the nanoscale. Such an understanding is essential for producing Au-Cu bimetallic nanoalloys with well-defined structural properties via wet chemical synthesis.

1. Introduction

In recent years, nanoscience and nanotechnology have grown extensively to such a point that nanomaterial study is nowadays a fast growing area of research. Among the wide range of nanosystems being studied, metallic nanoparticles (NPs) arouse considerable scientific and technological interests since they usually exhibit novel chemical and physical properties due to their much higher surface to volume ratio than bulk materials. The remarkable properties of metallic nanoparticles can be modified and finely tuned by adjusting their size, their shape and their composition. Pertaining to composition-dependent control of properties, several studies have shown that the association of two metals within a nanoparticle, i.e. forming bimetallic solids or so called nanoalloys, could lead to very important synergistic effects of interest in fields such as catalysis of industrially important reactions, optics, optoelectronics and medical applications[1].

Because of their potential impacts in the field of catalysis and optics and since they constitute a model bimetallic system, there has been immense interest in gold-copper (Au-Cu) nanoalloys. In heterogeneous catalysis, it has been shown that Au-Cu nanoalloys generally display synergistic effects in the oxidation and selective oxidation of carbon monoxide (CO) to carbon dioxide at ambient temperature[2,3], in the selective oxidation of benzyl alcohol to benzaldehyde[4] and in the epoxidation of propene by nitrous oxide[5] among others. More precisely, in the oxidation and the preferential oxidation of CO in excess of hydrogen, partially substituting gold with copper leads to an increase in activity as compared to monometallic Au NPs[2]. As for applications in nano-optics, it has been shown that by alloying copper into gold, the resulting Au-Cu NPs can display strong surface plasmon resonances (SPRs) with the copper content determining the energy and linewidth of the SPRs[6,7].

In bulk samples, gold and copper are completely miscible at any proportion at high temperature. At lower temperature, Au-Cu alloys form a tetragonal $L1_0$ superstructure for the AuCu stoichiometry and a cubic $L1_2$ superstructure for the Au_3Cu and $AuCu_3$ stoichiometries[8]. At the nanoscale, such a perfect knowledge of the phase diagram of Au-Cu alloy is still lacking. This limits the rational design of Au-Cu NPs for potential applications and for their study as a model system. Despite this major limitation, a broad range of preparation methods have been successfully implemented in recent years to synthesize Au-Cu nanosystems with various shapes and compositions[6,7,9-16]. Chemical methods have led to the production of Au-Cu NPs with spherical[7], pentacle[9], rod-like[6,10] and cubic shapes[11]. Pentacle gold–copper alloy nanocrystals with five-fold twinning in the size range from 45 to 200 nm have been recently synthesized by R. He *et al.* by a facile aqueous phase route involving the co-reduction of gold and copper salts[9]. Spatially-resolved X-ray spectroscopy elemental mapping confirms the formation of nanoalloys. The global Au content, measured by inductive coupled plasma-atomic emission spectroscopy, equals to 87.4 at. %.

Monodispersed pentagonal Au-Cu nanorods with controlled size and composition have also been developed by a seed-mediated growth route[10]. Likewise, Au-Cu nanocubes (NCs) with remarkable size control were synthesized by Y. Liu and A. R. H. Walker with a one-pot polyol reduction method[11], formerly developed by Fievet et al.[17]. By adjusting the reaction parameters, the authors claimed that they could control both the edge length between 3.4 nm to 85 nm and the particle composition between $AuCu_3$ and Au_3Cu. While it is indisputable that high shape and size control can be achieved by chemical methods, it is still unclear whether particle composition too can be tuned precisely. This results from the lack of systematic studies undertaken on chemically-grown Au-Cu NPs to determine their composition at single particle level and thus, to distinguish clearly between nominal and real compositions.

In comparison, physical methods offer better control of composition in the fabrication of bimetallic NPs. Au-Cu bimetallic NPs have been fabricated by ion implantation[12] or under ultra-high vacuum by thermal evaporation[13,14,15] and laser deposition[16]. For example, in the work of B. Pauwels *et al.*, Au-Cu nanoalloys were deposited on amorphous carbon and magnesium oxide substrates by laser vaporization of bulk alloy targets with different stoichiometric compositions (AuCu, $AuCu_3$ and Au_3Cu)[16]. By using electron diffraction on cluster assemblies and high-resolution transmission electron microscopy imaging of individual clusters, they showed that the Au-Cu clusters formed solid solutions with their chemical composition matching that of the target material. In the case of cluster deposition on amorphous carbon, various cluster morphologies such as cuboctahedra, decahedra and more spherical geometries were observed. For clusters deposited on MgO, only truncated octahedral morphologies were observed. As exemplified by this work, with physical techniques, high composition control is achieved in the absence of size and morphological homogeneity.

Herein, we first report the synthesis of Au-Cu NCs using a chemical route adapted from the polyol method developed by Y. Liu and A. R. H. Walker for producing cubic geometries[11] and the structural characterization of the as-synthesized NPs using transmission electron microscopy (TEM) techniques. TEM analysis undertaken at single particle level enables us to highlight and discuss the influence of reaction conditions such as the nominal amount of reactants on the NP structure. In the second part of this paper, the structural properties of Au-Cu NPs synthesized by pulsed laser deposition (PLD) are presented. Comparison of the morphology, size distribution, composition and crystal structure of chemically and physically synthesized NPs then allow us to better understand the reaction mechanisms which take place during the Au-Cu bimetallic nanoparticles synthesis by different routes.

2. Experimental

2.1 Preparation methods

Chemical syntheses of Au-Cu NCs were adapted from the polyol protocol described by Y. Liu and A. R. H. Walker[11]. Gold(III) chloride trihydrate ($HAuCl_4.3H_2O$; 99.9%), copper(II) acetylacetonate ($Cu(acac)_2$; 99.99%), 1,2-hexadecanediol (HDD; 90%), 1-dodecanethiol (DDT; 99%), 1-adamantane carboxylic acid (ACA; 99%), 1-hexadecylamine (HDA; 90%) and diphenylether (DPE; 99%) were purchased from Sigma-Aldrich and used without any further purification. In a typical chemical synthesis, $HAuCl_4.3H_2O$, $Cu(acac)_2$, HDD (1.6g; 6.19mmol), DDT, ACA (270mg; 1.50mmol), HDA (2g; 8.28mmol) were simultaneously introduced in a three-necked flask and dissolved in DPE (10mL). The amounts of metallic precursors and DDT were varied according to particles targeted composition. The mixture was stirred with a magnetic bar and refluxed at 180°C with a ramp of $8°C.min^{-1}$ under N_2 flow after 5 degassing cycles. After cooling to room temperature, the as-synthesized particles were collected and washed with 4 successive centrifugation runs (run 1 with chloroform ($CHCl_3$) and ethanol (C_2H_6O or EtOH) at 4,000 rpm during 5 min, run 2 with EtOH at 16,000 rpm for 10 min, run 3 with $CHCl_3$ at 16,000 rpm for 10 min and run 4 with dried acetone at 16,000 rpm for 10 min). The particles were finally dispersed in $CHCl_3$.

Au-Cu nanoparticles (NPs) were also produced by physical route via pulsed laser deposition (PLD) in a high-vacuum chamber at a pressure of about 10^{-7}mbar. This physical synthesis method is based on alternated irradiation of very high purity (99.9999%) Au and Cu monometallic targets by a KrF excimer Compex Pro 102F laser at 248 nm with a repetition rate of 5 Hz, pulse duration of 25 ns and energy between 125 and 500 mJ. Based on a continuous thin film approximation, deposition rate of each metal was controlled using an *in situ* quartz crystal monitor indicating the nominal thickness deposited on the quartz surface. Knowing the ablation rates of each metal, the composition and size of the nanoparticles can be precisely adjusted. The nanoparticles growth was performed at room temperature and home-made amorphous carbon TEM grids were used as substrate.

2.1 Characterization methods

For TEM grid preparation, an amorphous carbon film was first deposited on freshly cleaved mica in an Edwards Auto 306 evaporator pumped at a pressure of 10^{-6} mbar. A current range up to 10 A was applied to extract carbon atoms of the graphite stick. The amorphous carbon film was then delaminated from mica in water and transferred onto commercial molybdenum 300-mesh TEM grids (Agar Scientific). The carbon supports used were typically 4-5 nm thick which is ideal for Transmission Electrons Microscopy (TEM) studies of small metallic NPs. Aberration-free high-resolution transmission electron microscopy (HRTEM),

STEM high-angle annular dark-field (STEM-HAADF) and energy-dispersive X-ray spectroscopy (EDS) were carried out on a JEOL ARM 200F microscope, equipped with a cold field emission gun and a CEOS aberration corrector of the objective lens, operated at 200kV[18]. Particle composition was determined by energy dispersive X-ray spectroscopy on assemblies of NPs (TEM-EDS) and in scanning mode (STEM-EDS) on single NPs or assemblies. For these measurements, a beryllium sample holder was used to avoid spurious Cu X-ray emissions from the sample holder. Particle composition was determined by analyzing the intensities under the Au-$L_{\alpha,\beta}$ (9.71-11.44 keV range) and Cu-$K_{\alpha,\beta}$ (8.03-8.91 keV range) edges by the Cliff-Lorimer method[19] with an experimentally-determined K-factor.

3. Results and discussion

3.1 Structure of Au-Cu nanocubes synthesized by polyol protocol

In order to synthesize Au-Cu NCs with Au_3Cu and $AuCu_3$ nominal compositions, the ratio of metallic precursors was tuned as indicated in the Table 1. In these syntheses, the amount of Au precursor was kept fixed at 0.07 mmol and that of Cu precursor was varied accordingly to achieve the targeted compositions. The total amount of metallic precursors in the synthesis of $AuCu_3$ NCs was three times more important than that of Au_3Cu NCs. **Moreover**, the amount of DDT was also increased from 0.1 mL (for Au_3Cu NCs) to 0.3 mL (for $AuCu_3$ NCs) between the two syntheses. **The amounts of other reactants were kept unchanged. In these conditions, the concentration of metal ions was higher for the synthesis of $AuCu_3$ NCs than for Au_3Cu.** As a Figures 1a and 1b display low-magnification TEM images of Au-Cu NPs with Au_3Cu and $AuCu_3$ nominal compositions respectively. In these images, NPs with cubic in-plane morphologies are clearly evidenced. analyses of the two sets of NCs show that the average size of the NCs is 4.8 ± 1.3 nm in the sample with Au_3Cu nominal composition NCs (insert of figure 1a) whereas, owing to the increase of the metallic precursors amount from 0.10 mmol to 0.30 mmol, the $AuCu_3$ NCs have a mean size of 22.9 ± 1.5 nm (insert of figure 1b). As inferred from the comparison of TEM images in figures 1a and 1b, the polydispersity (mean particle size divided by the standard deviation) is about five times higher in the population of smaller NCs. To determine the structure of the NCs and the nature of their facets, high-resolution TEM imaging was performed on single NCs. Figures 1c and 1d show the HRTEM images of two NCs with Au_3Cu and $AuCu_3$ nominal compositions respectively. The corresponding fast Fourier transforms (FFTs) are displayed in the inserts and in both cases, they are consistent with chemically-disordered face-centered cubic (FCC) structures imaged along the [001] zone-axis and with major truncations along the [100] directions. Moreover, HRTEM images give clear evidence of cubic morphology of the as-synthesized NPs (figure S1).

To precisely characterize the shape of the NCs from each synthesized sample, the length (*L*), width (*W*) and diagonal (*D*) (figure 1c) of about 60 NCs from each synthesis batch were measured. The mean aspect ratio of each population was provided by calculating the averaged value of L/W ratio. Averaged L/W ratios of 1.06 ± 0.06 and 1.04 ± 0.02 were calculated respectively for the NC population with Au_3Cu and $AuCu_3$ targeted compositions. These results are then consistent with the cubic shape observed on the bright field images since each NPs population presented an average aspect ratio near to 1. Moreover, by comparing the experimentally-measured diagonal (*D*) to its theoretical value (D_{theo}) expected in the case of a perfect cubic shape, the truncation factor (*T*) of the NCs in each batch can be deduced via the following relation:

$$T = \frac{D_{theo} - D}{D_{theo}} \qquad (1)$$

whereby

$$D_{theo} = \sqrt{L^2 + W^2} \qquad (2)$$

T is equal to 0 for a non-truncated cube and its value increases toward 1 as the truncation increases. From the TEM image analyses, truncation factors of 0.22 ± 0.05 and 0.03 ± 0.02 were calculated for the Au_3Cu and $AuCu_3$ NCs population respectively. The near-zero truncation the $AuCu_3$ NCs is consistent with TEM images that show that they sustain sharper corners in comparison to Au_3Cu NCs.

STEM-EDS analyses of the NPs were performed to determine their real composition. Figure 2a shows the variation of Cu content as a function of particle size in the NCs with Au_3Cu nominal composition. No size-dependence is evidenced. The Cu content varies randomly between 6 and 23 at. % for sizes up to 8 nm with a mean composition equals to 11 ± 3 at. % Cu (insert of Figure 2a). A similar analysis undertaken on the NCs with $AuCu_3$ nominal composition shows again the absence of any relationship between size and composition and surprisingly, the NCs are rich in gold. Here, the composition is bound between 8 and 19 at. % Cu with an average composition of 12 ± 2 at. % Cu (Figure 2b). From composition analyses, it seems that the amount of copper content in alloyed Au-Cu NCs is limited to about 11-12 at. % Cu and thus, irrespective of the targeted composition, the real composition of the NC is always close to Au_8Cu. Such partial alloying between gold and copper has also been observed experimentally in earlier works[12,20,21] dealing with the synthesis of Au-Cu nanoalloys by chemical routes. However, the transformation of the non-alloyed copper ions was investigated in none of them. Here, in addition to nanocubes, STEM-HAADF investigations allow us to identify very small particles with an average size of 2 nm. Figure 3a displays a STEM-HAADF image of nanoparticles for the sample with $AuCu_3$ nominal composition in which these spherical NPs are clearly visible around NCs. STEM-EDS characterization of an assembly of these seeds over the region delimited by the green square in figure 3b, clearly demonstrates that they are pure copper nanostructures. For

comparison, an EDS spectrum acquired over a single Au-rich NC (over an area enclosed by the red square) is presented in Figure 3c. These results clearly illustrate that EDS characterization of a wide area of the samples would not only take into account the composition of NCs but would also include that of all the very small copper particles, leading to an overestimation of the real copper content of the nanocubes. Therefore, it is critically important to measure the composition of the synthesized NCs very locally such that the contribution of the spherical Cu seeds can be excluded. Our experimental observations tend to indicate that it is challenging to produce Au-Cu NPs with well-controlled composition via the bottom-up chemical method followed in this work.

The incomplete alloying of gold and copper in the Au-Cu NCs can be plausibly explained on the basis of the reactions kinetics associated with the chemical synthesis of these nanosystems. The synthesis of Au-Cu alloys via this method involves the following reactions:

$$Au^{3+}_{(aq)} + 3e^- \rightarrow Au^0_{(s)} \qquad (3)$$

$$Cu^{2+}_{(aq)} + 2e^- \rightarrow Cu^0_{(s)} \qquad (4)$$

The redox potential E°(Au^{3+}/Au) associated with reaction (3) equals to +1.50V[22]. For the reduction reaction of Cu ions, the corresponding potential E°(Cu^{2+}/Cu) is equal to +0.34V[22]. The redox potential of the reduction of Au(III) ions being higher than that of Cu(II) ions, it is likely that gold ions are more readily reduced in metallic Au(0) than copper ions in metallic Cu(0). Consequently, gold seeds might be formed and grown before all copper ions have been reduced, explaining the difficulty for gold and copper to form an alloy in the conditions used for chemical synthesis with these reactants.

3.2 Structure of Au-Cu nanoalloys synthesized by pulsed laser deposition

To study the interplay between gold and copper atoms at the nanoscale, pulsed laser deposition (PLD) which is a physical technique and bottom-up based too, was implemented to produce Au-Cu nanoalloys. PLD is well-established physical technique for the production of bimetallic nanoparticles with a high control in composition. In its first and most widely used approach, bimetallic nanoalloys are fabricated by vaporizing bulk alloy targets. In this case, the stoichiometries of the targets are reproduced in the nanoparticles. Using this approach, Au-Cu nanoalloys have been deposited on amorphous carbon and magnesium oxide substrates by ablating bulk AuCu, $AuCu_3$ and Au_3Cu targets[16]. In the present work, an alternative approach of PLD whereby Au-Cu NPs are obtained by the alternate ablation of pure gold and copper targets has been used. This approach has already been successfully applied to synthesize Co-Pt[23], Cu-Ag[24] and Au-Pd[25] nanoalloys and provides direct

information on the ability of atomic species coming from different sources to form nanoalloys.

In the present study, the production of Au_3Cu and $AuCu_3$ NPs was targeted. For all deposition, the nominal thickness of metal deposited was fixed to 1 nm. For the fabrication of Au_3Cu nanoalloys, the amount of gold and copper was, as indicated in table 2, equal to 0.75 nm and 0.25 nm respectively. The laser energy and the number of laser shots needed to ablate each metallic target are given alongside. For the synthesis of $AuCu_3$ nanoalloys, the laser conditions and respective amount of each metal were modified as described in table 2. It can be noticed that the laser energy needed to ablate gold is lower by about 100 mJ than that of copper. Moreover, despite the lower laser energy used, the ablation rate was much higher of gold than copper. As a result, number of laser shots on the gold target was much lower than on the copper ones.

Figures 4a-d present bright-field images of the two sets of Au-Cu NPs produced by PLD with targeted compositions Au_3Cu and $AuCu_3$. Low-magnification TEM images (figures 4a and 4b) clearly show the formation of well separated spherical NPs with comparable size distribution (mean diameter of 1.7 ± 0.6 nm (insert of figure 4a) in the Au_3Cu sample compared to 1.9 ± 0.7 nm (insert of figure 4b) in the $AuCu_3$ one) in both samples. HR-TEM images of a Au_3Cu and a $AuCu_3$ NPs are presented in figure 4c and 4d respectively. The NPs were monocrystals with FCC structure imaged along the [110] zone axis. To determine the lattice parameters of the two sets of NPs, the lattice spacing corresponding to (111) planes were measured on the HR-TEM images of 15 NPs from each sample. It should be noted that selected area electron diffraction (SAED) traditionally used for lattice measurements was impossible to implement in the present study. This is due to the very small dimension of the NPs which lead to extremely diffuse reflections in the SAED patterns acquired over particle assembly. From these lattice measurements, a mean lattice parameter equals to 3.99 ± 0.01 Å was estimated in the sample with Au_3Cu targeted composition. For the second sample, the mean lattice parameter was 3.74 ± 0.01 Å. The fact that these values lie between the lattice parameters of pure gold (a_{Au} = 4.078 Å) and pure copper (a_{Cu} = 3.610 Å) is a strong indication that the NPs deposited on home-made amorphous carbon by PLD are Au-Cu nanoalloys, with the sample with higher lattice parameter richer in gold. Moreover, from the very small dispersion in the values of the mean lattice parameters, it can be concluded that high composition homogeneity was achieved in each synthesis. To determine precisely the real particle composition obtained in each synthesis, assemblies of NPs over different areas of the two samples were analyzed by TEM-EDS with high counting statistics. From the analysis of the TEM-EDS spectra, the average Cu contents were 20 ± 1 at. % in the sample with Au_3Cu targeted composition (figure 4f) and 73 ± 3 at.% in the one with $AuCu_3$ targeted composition (figure 4f). It should be noted that to determine the exact composition distributions in the two samples, X-rays measurements at single particle level by STEM-EDS were initially undertaken. However, in this case, due to the small size of the NPs analyzed, the counting

statistics were so poor that determining particle composition with high precision was here impossible.

In bimetallic alloys, it has been reported that lattice parameter varies linearly with composition according to Vegard's law[26]. In Au-Cu alloy, the lattice parameter, *a,* of an alloy composed of *x* at. % Cu is given by $a = [x\ a_{Cu} + (100\text{-}x)a_{au}]/100$ if Vegard's law holds. Figure 5 shows a plot of the linear relationship between lattice parameter, *a,* and copper atomic content in Au-Cu alloy given by Vegard's law. The lattice parameter of the bimetallic alloy varies between that of the pure components. Two experimental data points are included in the plot of figure 5. The red point corresponds to the sample with mean lattice parameter equals to 3.74 ± 0.01 Å and composed of 20 ± 1 at. % Cu while the blue one is associated to the sample with mean lattice parameter equals to 3.99 ± 0.01 Å and composed of 73 ± 3 at.% Cu. **To test if the validity of Vegard's law is universal to all Au-Cu samples, the data points associated to the chemically synthesized NCs with Au_3Cu and $AuCu_3$ nominal composition were added to figure 5.** Within experimental uncertainties, it is clear that Vegard's law holds in both samples **obtained by chemical and physical syntheses** since the associated experimental points lie perfectly on the Vegard's curve. The validity of Vegard's law here makes it possible to uniquely determine the composition of any Au-Cu NP knowing its lattice parameter. This allows us to confirm a posteriori our assumption that particle composition was homogeneous in each sample, assumption based on lattice parameter measurements. Since the real compositions of the samples with Au_3Cu and $AuCu_3$ targeted composition are 20 at. % Cu and 73 at. % Cu respectively, pulsed laser deposition can be considered as a very efficient technique for the fabrication of disordered FCC Au-Cu nanoalloys with controlled composition. One of the advantages of the alternate PLD technique with pure metals targets is that any composition of an alloy can be aimed. Moreover, by modifying the ablation sequences, the synthesis of Au-Cu NPs with core-shell mixing pattern could also be possible via PLD.

4. Conclusion

In this paper, Au-Cu NPs were synthesized and their structural properties was studied by TEM. Firstly, cubic-shaped NPs with Au_3Cu and $AuCu_3$ nominal compositions were synthesized by a chemical route adapted from the polyol process. TEM imaging shows that NCs in a size range of 5 nm and 23nm were synthesized. These NCs presented a chemically-disordered face-centered cubic structure bounded by (100) facets. EDS measurements down to single particle level show that, irrespective of the targeted composition, the real compositions of the NCs were close to Au_8Cu. By using dark-field imaging, the presence of nanometer-sized pure copper NPs was also evidenced among the reaction products. This indicates that complete alloying of gold and copper is not achieved via the chemical method and reaction conditions implemented in this work. The incomplete alloying of Au and Cu is explained on the basis of the different redox potentials associated with the reduction of the

two metals from their salt precursors. In order to synthesize supported Au-Cu NPs with high control in composition, pulsed laser deposition (PLD) method was also developed. A 1-nm nominal thickness of metal was deposited on amorphous carbon with targeted compositions of Au_3Cu and $AuCu_3$. In both samples, Au-Cu monocrystals with FCC crystal structure and a size of about 2 nm were obtained. Lattice parameters determined experimentally on single NPs showed that the particle composition was homogeneous in each sample. **A high level of consistency with respect to Vegard's law was observed, showing that lattice parameter measurement can be used as a simple mean of determining the composition of Au-Cu nanoalloys.** These results clearly show that the composition of Au-Cu alloy nanoparticles can be easily controlled by pulsed laser deposition while, in the chemical synthesis by one-pot polyol method, the different reduction rates of the two metallic precursors hinders such control. A study is presently underway to produce Au-Cu nanoalloy with controlled composition using a two-pots chemical method in which the metals will be reduced separately before mixing. Nonetheless, chemical synthesis seems to be an appropriate method for Au-Cu nanoalloys since it can generate nanoparticles in greater quantities and with a fine-tuned shape.

Acknowledgements

We are grateful to Region Ile-de-France for convention SESAME E1845, for the support of the JEOL ARM 200F electron microscope installed at the Paris Diderot University. We thank Fernant Fiévet, Catherine Louis and Jolanda Spadavecchia for fruitful discussions and the Nanomaterials group of ITODYS laboratory at University Paris Diderot for their supports in the chemical synthesis.

References

1 R. Ferrando, J. Jellinek and R. L. Johnston, *Chem. Rev.*, 2008, **108**, 845–910.
2 X. Liu, A. Wang, T. Zhang, D.-S. Su and C.-Y. Mou, *Catal. Today*, 2011, **160**, 103–108.
3 D. I. Potemkin, E. Y. Semitut, Y. V. Shubin, P. E. Plyusnin, P. V. Snytnikov, E. V. Makotchenko, D. Y. Osadchii, D. A. Svintsitskiy, S. A. Venyaminov, S. V. Korenev and V. A. Sobyanin, *Catal. Today*, 2014, **235**, 103–111.
4 C. Della Pina, E. Falletta and M. Rossi, *J. Catal.*, 2008, **260**, 384–386.
5 R. J. Chimentão, F. Medina, J. L. G. Fierro, J. Llorca, J. E. Sueiras, Y. Cesteros and P. Salagre, *J. Mol. Catal. Chem.*, 2007, **274**, 159–168.
6 A. Henkel, A. Jakab, G. Brunklaus and C. Sönnichsen, *J. Phys. Chem. C*, 2009, **113**, 2200–2204.
7 N. E. Motl, E. Ewusi-Annan, I. T. Sines, L. Jensen and R. E. Schaak, *J. Phys. Chem. C*, 2010, **114**, 19263–19269.
8 H. Okamoto, D. J. Chakrabarti, D. E. Laughlin and T. B. Massalski, *J. Phase Equilibria*, 1987, **8**, 454–474.
9 R. He, Y.-C. Wang, X. Wang, Z. Wang, G. Liu, W. Zhou, L. Wen, Q. Li, X. Wang, X. Chen, J. Zeng and J. G. Hou, *Nat. Commun.*, 2014, **5**.

10 J. Yang, L. L. Chng, X. Yang, X. Chen and J. Y. Ying, *Chem. Commun.*, 2014, **50**, 1141.
11 Y. Liu and A. R. H. Walker, *Angew. Chem.*, 2010, **122**, 6933–6937.
12 G. Battaglin, E. Cattaruzza, F. Gonella, G. Mattei, P. Mazzoldi, C. Sada and X. Zhang, *Nucl. Instrum. Methods Phys. Res. Sect. B Beam Interact. Mater. At.*, 2000, **166–167**, 857–863.
13 A. Wilson, R. Bernard, A. Vlad, Y. Borensztein, A. Coati, B. Croset, Y. Garreau and G. Prévot, *Phys. Rev. B*, 2014, **90**, 075416.
14 H. Yasuda and H. Mori, *Z. Für Phys. At. Mol. Clust.*, 2014, **37**, 181–186.
15 H. Yasuda, H. Mori, M. Komatsu and K. Takeda, *Appl. Phys. Lett.*, 1992, **61**, 2173–2174.
16 B. Pauwels, G. Van Tendeloo, E. Zhurkin, M. Hou, G. Verschoren, L. Theil Kuhn, W. Bouwen and P. Lievens, *Phys. Rev. B*, 2001, **63**, 165406.
17 F. Fievet, J. P. Lagier, B. Blin, B. Beaudoin and M. Figlarz, *Solid State Ion.*, 1989, **32–33, Part 1**, 198–205.
18 C. Ricolleau, J. Nelayah, T. Oikawa, Y. Kohno, N. Braidy, G. Wang, F. Hue, L. Florea, V. P. Bohnes and D. Alloyeau, *Microscopy*, 2013, **62**, 283–293.
19 G. Cliff and G. W. Lorimer, *J. Microsc.*, 1975, **103**, 203–207.
20 G. De and C. N. R. Rao, *J. Phys. Chem. B*, 2003, **107**, 13597–13600.
21 J. Llorca, M. Domínguez, C. Ledesma, R. J. Chimentão, F. Medina, J. Sueiras, I. Angurell, M. Seco and O. Rossell, *J. Catal.*, 2008, **258**, 187–198.
22 A. J. Bard, R. Parsons and J. Jordan, *Standard Potentials in Aqueous Solution*, CRC Press, 1985.
23 D. Alloyeau, C. Langlois, C. Ricolleau, Y. L. Bouar and A. Loiseau, *Nanotechnology*, 2007, **18**, 375301.
24 C. Langlois, Z. L. Li, J. Yuan, D. Alloyeau, J. Nelayah, D. Bochicchio, R. Ferrando and C. Ricolleau, *Nanoscale*, 2012, **4**, 3381.
25 J. Nelayah, N. T. Nguyen, D. Alloyeau, G. Y. Wang and C. Ricolleau, *Nanoscale*, 2014, **6**, 10423.
26 L. Vegard, *Z. Für Phys.*, 1921, **5**, 17–26.

Tables/Figures:

Targeted composition	$Cu(acac)_2$ (mmol)	$HAuCl_4.3H_2O$ (mmol)	Cu (II) :Au (III)
Au_3Cu	0.03	0.07	0.43
$AuCu_3$	0.23	0.07	3.29

Table 1: Amount of metallic precursors used in the synthesis of NCs with Au_3Cu and $AuCu_3$ nominal compositions. The respective Cu (II): Au (II) ratios are also given.

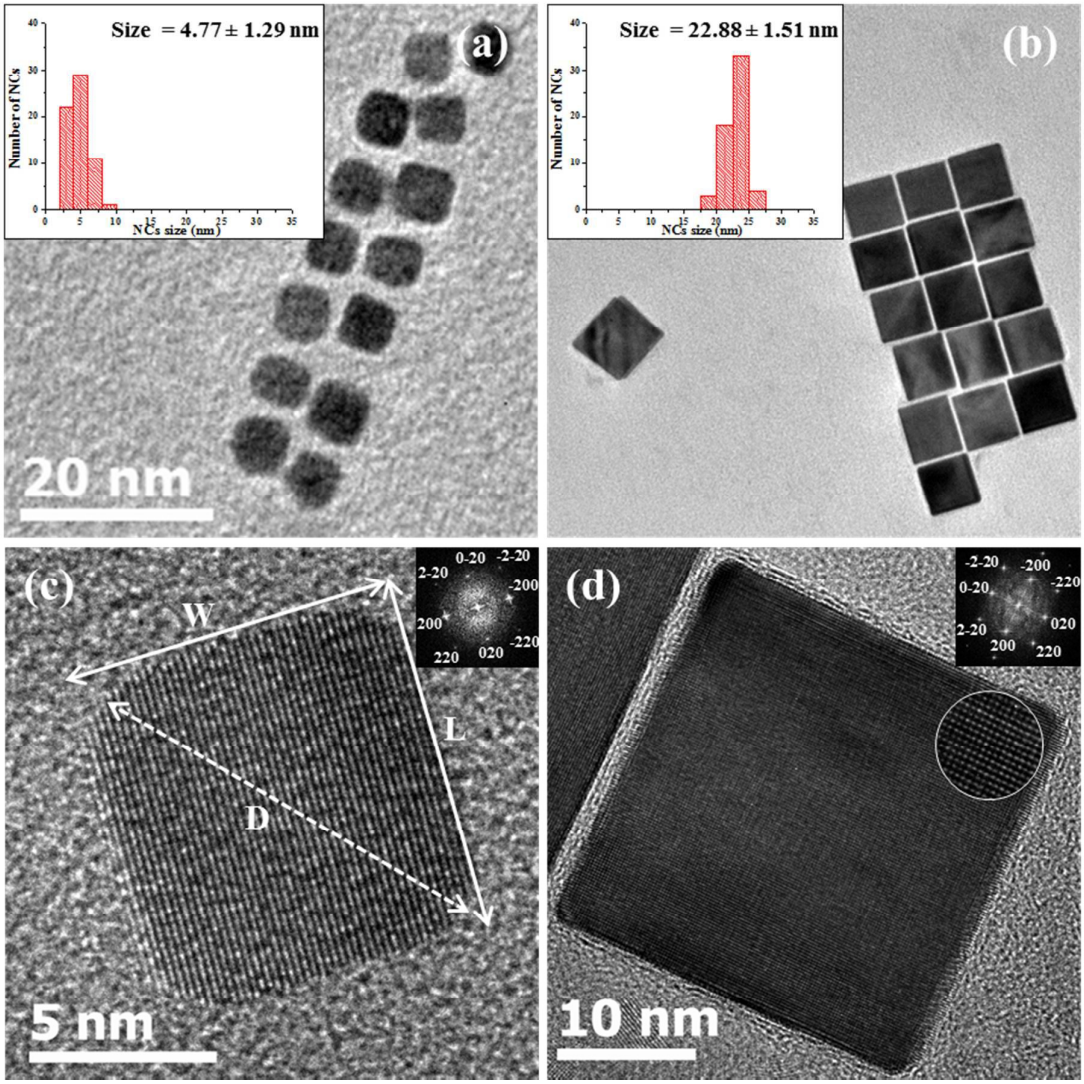

Figure 1: (a) and (b) Bright-field low-magnification images of Au-Cu NCs with Au_3Cu and $AuCu_3$ nominal compositions respectively. The corresponding size distributions are presented in insert of images. (c) and (d) High-resolution imaging of the Au_3Cu and $AuCu_3$ nominal compositions NCs from which FFT have been extracted in insert. Length (L), width (W) and diagonal (D) have been represented in image (c).

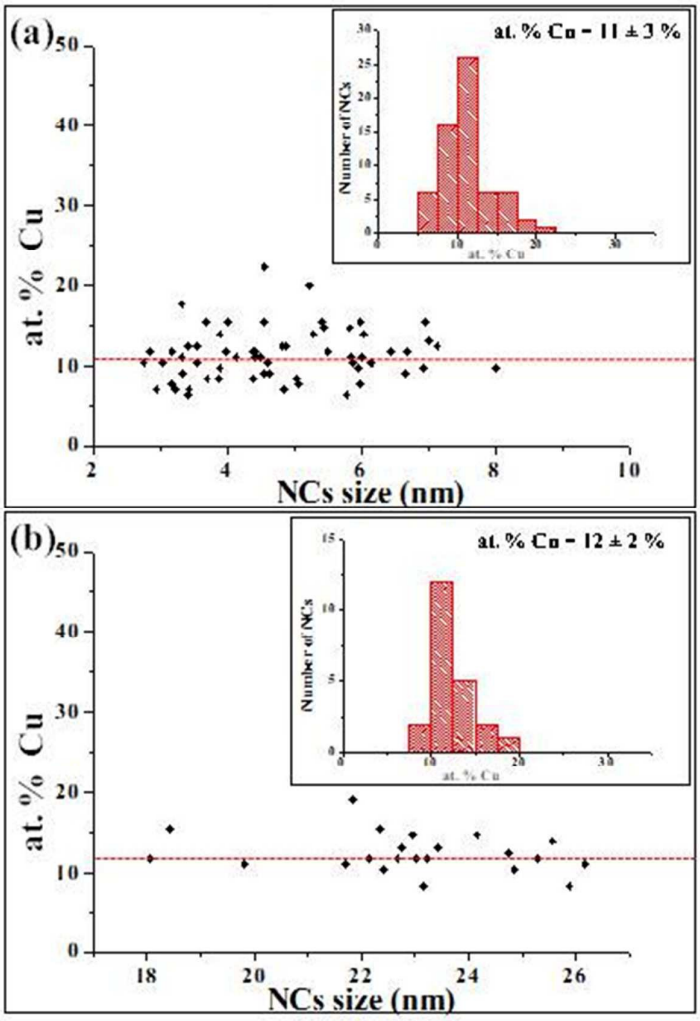

Figure 2: Statistical study of the copper content as a function of particle size for (a) Au_3Cu and (b) $AuCu_3$ nominal compositions. The mean copper contents in each sample are indicated by red broken lines. In inserts, the respective composition distributions are shown.

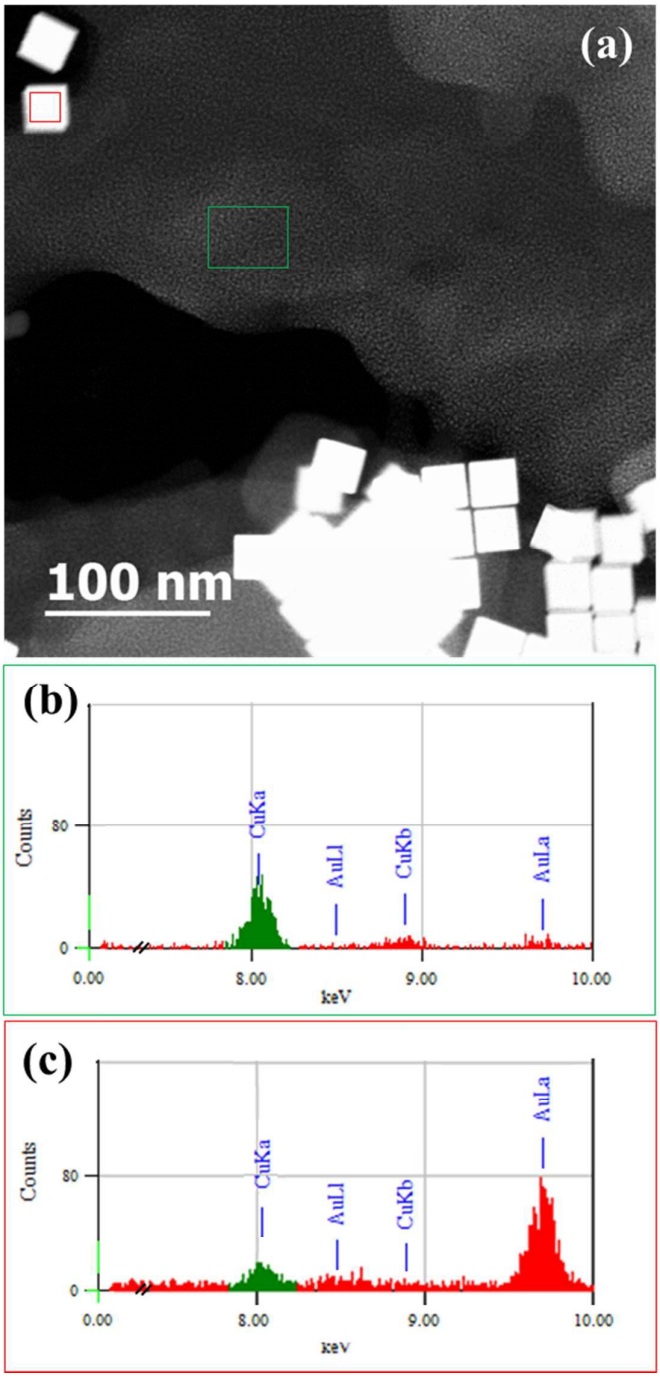

Figure 3: (a) Dark-field image of $AuCu_3$ nominal composition NCs surrounded by small copper nanoparticles. The green and red squares delimit the areas whose respective EDS spectra are presented in (b) and (c).

Targeted composition	Material	N.T. (nm)	Energy (mJ)	Number of shots
Au_3Cu	Au	0.75	388	108
	Cu	0.25	279	330
$AuCu_3$	Au	0.25	380	42
	Cu	0.75	290	1542

Table 2: PLD synthesis parameters for the fabrication of Au_3Cu and $AuCu_3$ NPs.

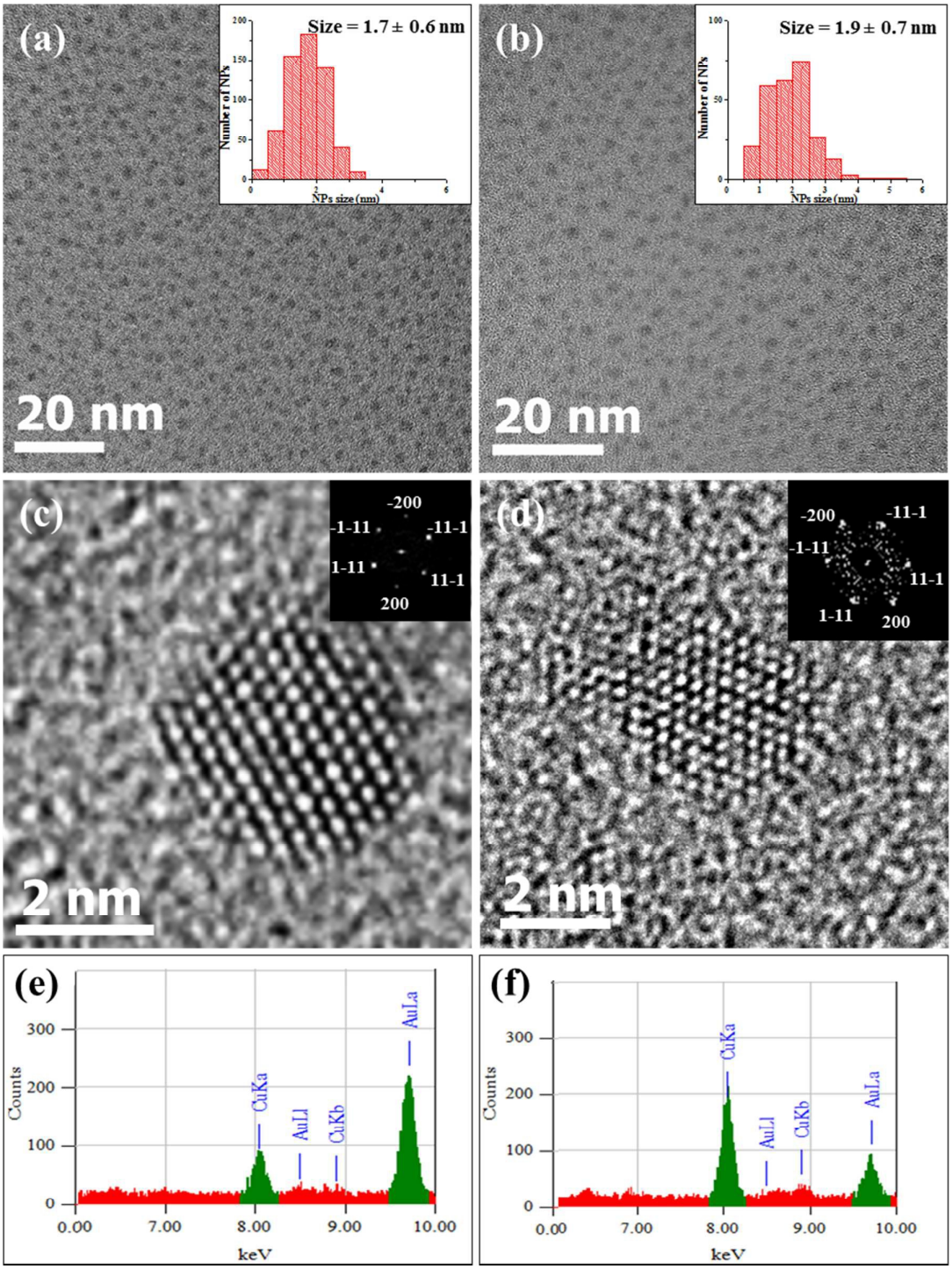

Figure 4: (a) and (b) Bright-field low-magnification images of NPs with a nominal composition of Au_3Cu and $AuCu_3$ respectively. The corresponding size distributions are presented in insert of images (a) and (b); (c) and (d) High-resolution imaging of the Au_3Cu and $AuCu_3$ NPs from which FFT have been extracted in insert. (e) and (f) TEM-EDS spectra acquired on assemblies of Au_3Cu and $AuCu_3$ NPs

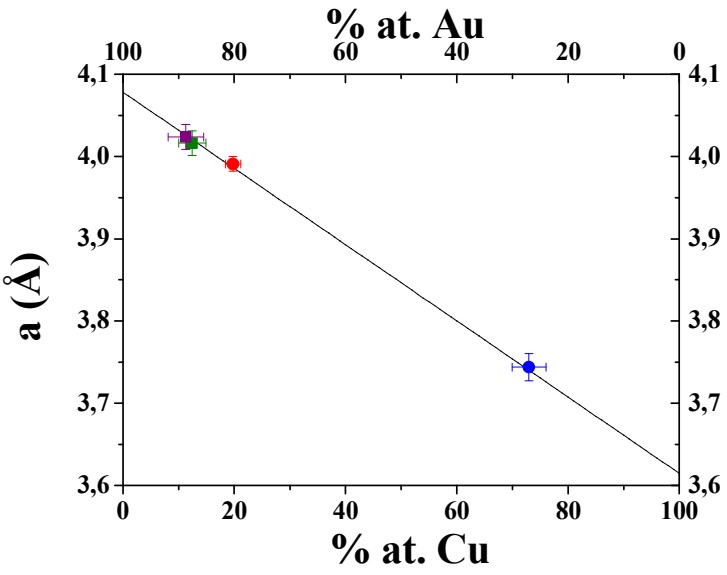

Figure 5: Lattice parameter of the NPs as a function of the atomic composition. Red and blue **circles** correspond respectively to the mean lattice parameter and mean composition of the samples with Au_3Cu and $AuCu_3$ nominal compositions **obtained by PLD**. **The mean lattice parameter and mean composition of NCs with Au_3Cu and $AuCu_3$ nominal compositions obtained by chemical synthesis are also indicated by purple and green squares respectively**. For comparison, the Vegard law has been plotted in black line.